
Proceedings Paper:
Priest, J., Ghadbeigi, H., Ayvar-Soberanis, S. et al. (1 more author) (2021) Effects of coefficient of friction coupled with a deformation dependent friction model in cutting simulations. In: Govekar, E., Pušavec, F. and Vrabic, R., (eds.) Procedia CIRP. 8th CIRP Conference on Modeling of Machining Operations (CMMO), 15-17 Jun 2021, Ljubljana, Slovenia (online). Elsevier , pp. 429-434.

https://doi.org/10.1016/j.procir.2021.09.073

Available online at www.sciencedirect.com

ScienceDirect

Procedia CIRP 102 (2021) 429–434

www.elsevier.com/locate/procedia

18th CIRP Conference on Modeling of Machining Operations

Effects of coefficient of friction coupled with a deformation dependent friction model in cutting simulations

Joshua Priest[a,b], Hassan Ghadbeigi*[a], Sabino Ayvar-Soberanis[c], Anders Liljerehn[d]

[a] Department of Mechanical Engineering, Sir Frederick Mappin Building, The University of Sheffield, Sheffield, S1 3JD, UK
[b] Industrial Doctoral Centre in Machining Science, Advanced Manufacturing Research Centre with Boeing, University of Sheffield, Rotherham, S60 5TZ, UK
[c] Advanced Manufacturing Research Centre with Boeing, University of Sheffield, Rotherham, S60 5TZ, UK
[d] Sandvik Coromant AB, Gavleborg, Sweden

* Corresponding author. Tel.:+44 (0)114 222 7748; fax: N/A. *E-mail address:* h.ghadbeigi@sheffield.ac.uk

Abstract

A deformation dependent stick-slip based friction model is realised to better represent the contact stresses in the secondary shear zone. The instantaneous nodal limiting shear stress is implemented in a VFRIC friction model subroutine in ABAQUS\Explicit in 2D ALE orthogonal cutting simulations to investigate effects on the accuracy of the simulations. This study highlights that the limiting shear stress varies along the rake face, as well as with the rake angle and uncut chip thickness. Lower coefficients of friction are necessary at lower rake angles and higher uncut chip thicknesses, although a variable coefficient of friction model is still necessary to predict both the cutting force and thrust force accurately together.

Keywords: Machining;Friction;Modelling

1. Introduction

Accurately modelling the frictional forces between the tool-chip and the tool-workpiece contact is critical in machining simulations as this impacts the cutting forces, chip formation, resultant surface integrity of the machined surface, and the rate of tool wear [1]. These frictional interactions are complex primarily due to the high normal contact pressures, temperatures, and sliding speeds [2]. Most of the friction models implemented in simulation of chip formation are based on the Coulomb friction law [3], [4] and the stick-slip model developed by Zorev where the frictional shear stress is limited to the upper bond approximation of the shear strength of the material and evidence of which is already reported in the literature [5]. this accounts for the elastic (sliding) and plastic (sticking) contact regime within the secondary deformation zone where the coefficient of friction (COF) and frictional shear stress play crucial role [6]–[8]. This limiting shear stress, like the COF, is heavily dependent on the local deformation conditions and temperature [9].

However, the coupling of limiting shear stress with flow property of the material at the contact point has been rarely reported, e.g. Refs [2], [10]–[12] in the literature for simulation of chip formation. This is commonly assumed as a constant value [2]. Although velocity and temperature dependent friction model have already developed for simulation of machining [13], [14] and forming [15] processes these are not directly coupled with the friction models sensitive to local material properties at the contact point between the tool and the chip.

Friction models are reported to have 25% higher impact on the predicted feed force than the cutting force [6]. While most of the simulation results in the literature are validated against the cutting force or the chip geometry there is always large discrepancies in the predicted thrust forces compared with the experimentally measured values. This could be linked to the low friction coefficients (between 0.2 – 0.6 across a range of materials [16]) or ignoring the effect of plastic deformation on the material in the secondary deformation zone contacting the tool rake face affected by the applied limiting shear stress in the

10.1016/j.procir.2021.09.073

models. The latter can only be calibrated observing the shearing and plastic deformation in this zone directly ahead of the tool that is almost impossible due to the severity of the deformation condition and image processing techniques such as Digital Image Correlation [17], [18] cannot resolve the deformation.

The stick-slip model has been shown to be more representative of the shear frictional stress distribution than the Coulomb models on the tool rake face, yet these have been shown in studies of orthogonal cutting to be slightly less accurate [2]. Therefore, more development in friction modelling is required. Aside from the choice of model, it has been shown that the correct calibration of the coefficients of friction and the limiting shear stress in the stick-slip models significantly impact the prediction accuracy. It is already reported that the friction coefficient could be linked to the applied rake angle and other cutting parameter [16], however the effect of this dependency on the predicted process outputs has not been investigated.

In the present research a systematic study has been conducted to investigate the variation of the friction coefficient and limiting shear stress distribution in the secondary shear zone with the rake angle and the uncut chip thickness during orthogonal cutting of AA2024-T351 while the frictional shear stress is coupled with the local material properties. This is the first time, to the best knowledge of the authors, that the frictional limiting shear stress is coupled with the local deformation conditions in order to study the variation of the friction coefficient and frictional shear stress distribution in the secondary shear zone in detail. Although the microgrids technique has been previously used to determine deformation field with in the primary deformation zone and at the machined surface, this research is for the first time reports on characterization of deformation within the secondary deformation zone and at the vicinity of the tool rake face in order to determine the realistic friction coefficient responsible for the measured deformation field.

2. Experimental Setup

A complete set of experimental data is required for this research that included cutting and thrust forces, chip morphology under a variation of uncut chip thicknesses and rake angles. Therefore, the available experimental results for orthogonal cutting of AA2024-T351 from List et al. [19] was selected.

Additionally, low speed linear orthogonal cutting tests were carried out to quantify local deformation fields where two blocks of 25mm by 25mm with 5mm thickness were used. The contacting surface of the samples were prepared with a mirror polish and microgrids of 10µm pitch were printed on the polished side of one of the blocks using electron beam lithography as explained in [21]. The tests were carried out with a cutting speed of 2.4m/min, a rake angle of 7° and the uncut chip thickness of 0.25mm and 0.5 mm and interrupted by rapid disengagement of the cutting tool to preserve plastic deformation in the primary deformation zone (PSZ) and the secondary deformation zone (SDZ). Higher cutting speeds are not achievable due to limitations of the equipment and technique used to rapidly disengage the tool in this study.

3. Modelling Methodology

Thermo-mechanically coupled Finite element models of the orthogonal cutting were developed in Abaqus/Explicit using Arbitrary Lagrangian Eulerian (ALE) formulation with second order advection to preserve initial mesh bias and sizes. Two sets of simulations were conducted to study the effect of rake angle variations and friction coefficient on the accuracy of predicted cutting forces and measured deformation fields in machining of AA2024-T351. The workpiece material was developed with a predefined chip geometry and CPE4RT thermally coupled reduced integration elements in the chip formation zones were used to mesh the Eulerian domain. Fig. 1 shows a schematic of the developed model together with the applied boundary conditions wherein the cutting tool is modelled as a rigid body with thermal properties.

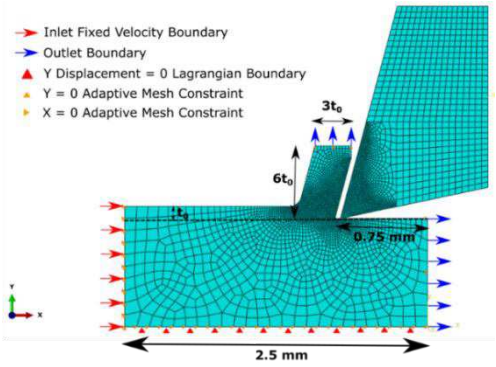

Fig. 1. Model geometry with red arrows indicating the Eulerian inflow boundaries.

The workpiece material behavior was modelled using the Johnson-Cook (JC) constitutive equation and it was assumed that 90% of the mechanical work and all the frictional energy are converted to heat that is equally partitioned between the workpiece and the cutting tool. An additional contact conductance of 200 kW/m^{2}K was used to describe the thermal conduction between the tool and the chip as determined experimentally for the used cutting conditions [20]. Table 1 shows the mechanical and physical properties of the cutting tool and the workpiece material implemented in all the simulations. The applied cutting parameters and tool geometry variations in each simulation sets are described in Table 2. In the first set of modelling, the cutting speed was kept constant at 60m/min and the rake angle was varied, then in the second set of modelling results the uncut chip thickness was increased to 0.3 mm whilst the speed and rake angle were kept constant at 60m/min and 15°, respectively. The experimentally measured cutting and thrust forces in [21] were used to compare the models performance.

The kinematic contact algorithm together with a user subroutine (VFRIC) was used to describe the stick-slip frictional condition according to, equation (1), where the Coulomb friction model is used to calculate the frictional shear stresses (τ_f) in an elastic slipping contact (where σ_n is the contact pressure), and the local nodal limiting shear stress (τ_y) is used to limit this frictional stress in plastic sticking region. The local stresses calculated at the integration points of the elements were used to determine stresses at the contacting

nodes within the developed (VFRIC) user subroutine to better represent stress state at the contacting bodies. These local limiting shear stresses were calculated in the subroutine as shown in equation (2) as limitations of the ALE mesh formulation meant history-dependent variables, such as the plastic strain rate, could not be accurately calculated. At plastic strains (ε_p) above "0" the material is assumed to be actively yielding so the flow stress is equivalent to the strain rate, temperature and plastic strain dependent von-Mises equivalent stress ($\bar{\sigma}$). At plastic strains below "0", the stress is calculated using the reduced form of the Johnson Cook constitutive model to only consider temperature dependent term at the yield point. The friction model application and nodal interpolation of integration point values components of the subroutine were validated separately by comparing each component to the GUI implementation.

Table 1. Physical and mechanical properties of the workpiece material and cutting tool [22].

JC parameters		Mechanical/Physical properties		
A (MPa)	265	Young's modulus, E (GPa)	AA2024-T351	73
B (MPa)	426		Tool	630
C	0.015	Poisson's ratio, ν	AA2024-T351	0.33
m	1		Tool	0.23
n	0.34	Density, ρ (kg/m³)	AA2024-T351	2,780
$\dot{\varepsilon}_0$ (s-1)	1		Tool	15,000
T_{room} (K)	293	Conductivity, k (W/mK)	AA2024-T351	120
T_{melt} (K)	775		Tool	100
		Specific heat, cp (J/kgK)	AA2024-T351	856
			Tool	240

$$\tau_f = \begin{cases} \mu\sigma_n, & \mu\sigma_n < \tau_y \\ \frac{\bar{\sigma}}{\sqrt{3}}, & \mu\sigma_n \geq \tau_y \end{cases} \quad (1)$$

$$\tau_y = \begin{cases} \frac{[A]\left[1-\left(\frac{T-T_0}{T_m-T_0}\right)^m\right]}{\sqrt{3}}, & \varepsilon_p < 0 \\ \frac{\bar{\sigma}}{\sqrt{3}}, & \varepsilon_p > 0 \end{cases} \quad (2)$$

This was also further validated by re-creating the model by Atlati [22] which also implement a variable limiting shear stress model with minimal discrepancy of less than 5% for both cutting force and thrust force predictions.

Table 2. Cutting parameters and tool geometry used in the simulations

Cutting speed, v_c (m/min)	2.4	60
Uncut chip thickness, *h* (mm)	0.25; 0.5	0.1, 0.3
Rake angle, γ (°)	7	0; 15; 30
Clearance angle, α (°)	12	7
Cutting edge radius, *r* (μm)	10	10
Friction Coefficient (μ)	0.2; 0.4; 0.6; 0.8; 1; 1.2; 1.4	

In the third set of modelling, the slow speed cutting conditions, described in section 2, were modelled across a range of coefficients of friction up to 0.4. To account for the deformation mechanics at the slower (2.4 m/min) cutting speed. The required parameters Johnson Cook constitutive and damage model parameters for the used material in these cutting tests, Table 3, were determined. Neglecting the damage consideration at these lower cutting speeds resulted in model instability and failure.

Only the 0.25 mm uncut chip thickness condition was successfully modelled as the 0.5 mm uncut chip thickness produced a significantly segmented chip in the experiment (Fig 2b) which cannot be accurately predicted by the ALE with Eulerian boundaries modelling methodology used.

Table 3. JC parameters for the slow cutting speed simulations.

JC Constitutive Parameters		JC Damage Parameters	
A (MPa)	350	d1	0.12
B (MPa)	675	d2	0.1
C	0.0085	d3	-1.7
m	1	d4	0.011
n	0.57	d5	0
$\dot{\varepsilon}_0$ (s-1)	0.0013		
T_{room} (K)	293		
T_{melt} (K)	775		

4. Results and Discussions

4.1. Secondary shear zone deformation characterisation

The in-situ cutting trials generated semi-continuous chips where the shear localisation increased with the uncut chip thickness as expected. Fig. 2 shows the micrographs of the chip sections together with the grid patterns used to measure the local deformation field. The local deformation in the PDZ and SDZ where measured according to the finite plastic deformation theory using the deformed configurations of the grid lines. Fig. 3a and b shows the plastic equivalent strain maps within the PDZ of samples cut with 0.25 and 0.5mm uncut chip thicknesses while the strain maps within one chip segment of the latter is shown in Fig 3c. The maps of Fig 3 indicate that material experiences plastic strains as high as 1.3 before the onset of shear localisation within PDZ leading to the chip segmentation and the cyclic deformation pattern as it is observed in Fig. 3c.

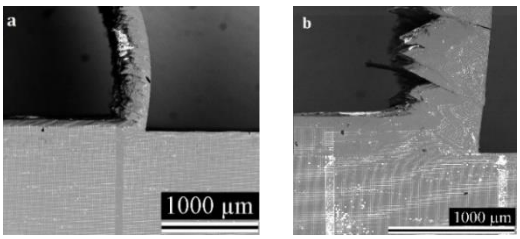

Fig. 2. Chip section of machined samples at 2.4m/min with (a) 0.25 mm and (b) 0.5mm uncut chip thickness

Although the DIC technique has recently been used to determine the evolution of deformation during chip formation, the resolution of optical systems used restricts the accurate deformation measurement within critical regions ahead of the tool rake face. The applied technique here helps to quantify machining induced deformation as close as few microns to the rake face as demonstrated by the highlighted grid lines (1-7) in Fig. 3a and 3c. The lines follow the deformed horizontal grid lines where the distance of adjacent lines was equal to the grids pitch (10 μm). The imposed deformation cannot be quantified accurately due to very severe distortion of the grids, however variations of the grids lines spacing indicates the extent of deformation experienced by the material.

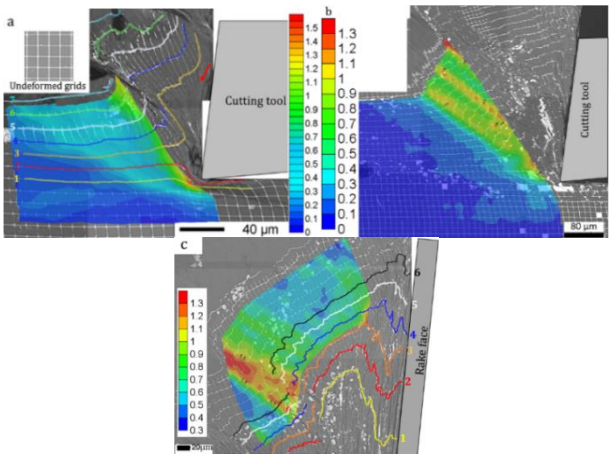

Fig. 3. Distribution of measured equivalent plastic strain at the chip section in orthogonal cutting with 2.4m/min cutting speed and a uncut chip thickness of (a)0.25mm and (b,c) 0.5mm.

The distorted grid lines in Fig.3a indicates that the deformation increases drastically for the material closer to the rake face as lines 6, 5, and 3 are further separated with a maximum extension of 178% in the grids length. A stagnation point was formed between lines 2 and 3 where the material along the red line is pushed under the tool nose radius while a nominal logarithmic strain values above 6 could be expected within the SDZ in the applied cutting conditions as indicated by the excessively distorted grids shown by the red arrow in Fig. 3a. As the uncut chip thickness increases, material in chip section experiences a complex deformation in the sticking region (shown by lines 1-4 in Fig. 3c) involving a very large compression on the rake face with up to about 75% reduction in the grids width within the 20 µm proximity of the rake face. The highlighted lines shows a transition in the material flow pattern due to the changes in the frictional condition and chip segmentation mechanisms. At the early stages of segmentation due to the sticking friction the nominal logarithm strain is as high as 2.2 (points 1 and 2 along the rake face) while as the material slides over it reduces to about 1.6 (between points 2 and 3) close to the maximum strain observed in the localised shear zone (~ 1.4). The measured strain values at vicinity of the tools' rake face shows not only the friction condition changes by the rake angles, but also a constant friction coefficient will not truly represent the tribological condition of the highly deformed material with a very large deformation gradient along the rake face.

The observed variations of local compressive, shear and tensile deformations along the rake face, makes a localised shear stress limit necessary for the friction modelling along the rake face. This should also be coupled with the flow properties of the material given the complex deformation history observed from PDZ to the SDZ.

4.2. Rake angle and uncut chip thickness effects on friction coefficient and modelling accuracy

The differences in predicted results are plotted against the applied friction coefficient for variation of rake angles in Fig. 4 and for the variation of uncut chip thickness in Fig 5. The red dashed lines show the cutting force data while the solid lines correspond to the thrust force prediction accuracy. As the rake angels increases, the predicted forces become less sensitive to the variations of friction coefficient which is linked to the plastic sticking length gradually increasing with COF and approaching the full contact length as demonstrated in Fig.6a. Fig 6a demonstrates the lower rake angles are the most sensitive as the ratio of plastic sticking to elastic sliding contact on the rake face is smaller. The COF that yields the most accurate result progressively increases with the positive rake angle, and the results indicate that higher coefficients of friction are required to accurately predict the thrust force compared to the cutting force. These values also do not always correlate with the apparent coefficient of friction as shown in Fig.4.

Fig.5 shows that lower COF values are required to more accurately predict the thrust force at higher uncut chip thicknesses, although there is a minimal change in the response of the cutting force error with varying COF.

These graphs (Fig.4 and Fig.5) indicate that although an accurate prediction of both the cutting and thrust forces is not possible using a constant friction coefficient, an optimised value can be used to reach a reasonable accuracy with less than 20% error in both values in various deformation conditions. Fig. 4 also shows despite the coupling of the limit shear stress with the local properties of the material, variation in local deformation field and material properties along the rake face, as shown in Fig. 3, requires a more complex friction coefficient model to accurately describe the contact conditions where there exist large deformation and stress gradients.

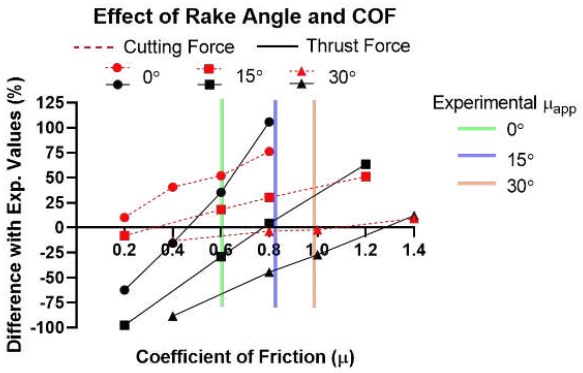

Fig. 4. Variation of modelling error with COF across rake angles from 0 to 30°. Green, blue, and orange vertical solid lines represent the experimental apparent COF values.

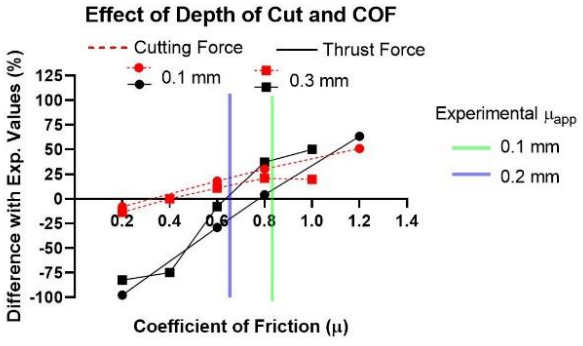

Fig. 5. Variation of modelling error with COF for 0.1 mm and 0.3 mm uncut chip thickness with a constant rake angle of 15°. Green and blue vertical solid lines represent the experimental apparent COF values.

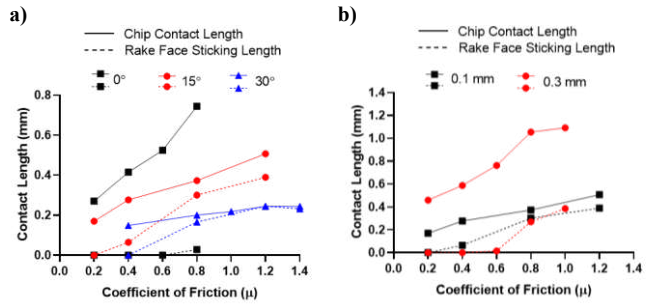

Fig. 6. The effect of the rake angle (a) and the uncut chip thickness (b) on the chip contact lengths (shown by solid lines) and the rake face sticking zone length (shown by dashed lines).

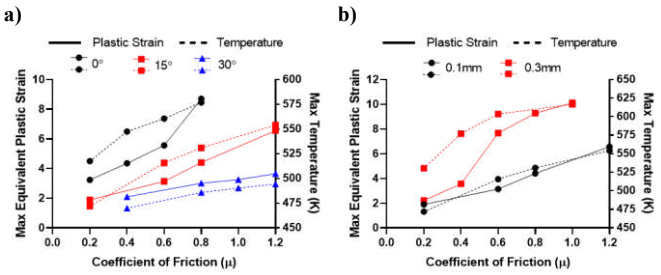

Fig. 7. Predicted maximum equivalent plastic strain and temperature in SDZ with varying COF for the rake angles (a) and uncut chip thicknesses (b).

The limiting shear stresses variation along the rake face and the edge of the tool are shown in Fig.8a and 8b (graphs start at the cutting edge) comparing the rake angle and uncut chip thickness effect, respectively. The limiting shear stresses at the rake face were not significantly affected by the COF value. The limiting shear stress at the cutting edge of the tool progressively decreases from about 350 MPa to 275MPa as the rake angle decreases from 30° to 0°, respectively. This is due to the reduced thermal softening at higher rake angles, shown in Fig 7a. The increased uncut chip thickness (at a 15° rake angle, Fig 8b) does not affect the limiting shear stress around the nose radius of the cutting edge. However, there is a drop of about 20% in the limiting shear stress further up the rake face at the higher uncut chip thickness that is linked to increased thermal softening on the rake face at higher uncut chip thicknesses as demonstrated in Fig 7b; this significant reduction is not seen at the lower uncut chip thickness because of the smaller tool-chip contact length as shown in Fig.6b and reduced frictional work converted to heat. Therefore, the limiting shear stress is not constant and is varying with the tool geometry and cutting conditions.

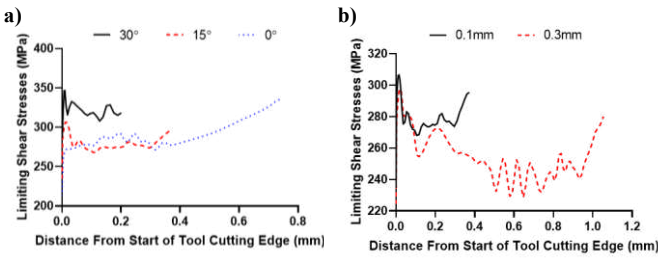

Fig. 8. The effect of the rake angle (a) and the uncut chip thickness (b) on the limiting shear stresses along the cutting edge and rake face of the tool.

Additionally, these shear stress limits across all the conditions tested are between 37% and 56% higher than the limiting shear stress (153MPa), commonly calculated using the reference uniaxial yield strength ($A/\sqrt{3}$), seen in Table 1. Therefore using a constant material-only dependent limiting shear stress would under-predict the shear stresses on the rake face, reduce the predicted thrust forces, and reduce the predicted cutting forces at rake angles above 0°.

4.3. Slow speed cutting deformation conditions prediction accuracy

Fig. 9 shows the equivalent plastic strain maps of the slow cutting speed at 0.25mm uncut chip thickness. The local deformation at the shear plane (~1) and the proximity of the rake face (~6) is better predicted with the COF of 0.4 compared with the measured experimental results in Fig. 3a while the cutting force prediction is within 14% error of the experimentally measured values.

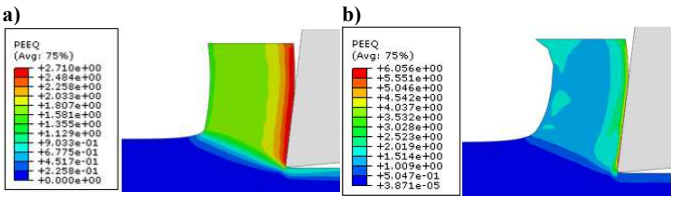

Fig. 9. The predicted plastic equivalent strain of the slow cutting speed model at 0.25mm uncut chip thickness with a COF of (a) 0.2 and (b) 0.4.

In contrast to the previous models where the limiting shear stress was not affected by the COF, it is very sensitive to the COF in the current models, Fig.10, as material softening due to damage initiation and propagation was implemented. Increasing the COF from 0.2 to 0.4 resulted in about a 50% reduction in the limiting shear stress that highlights the need for a lower COF values when using a deformation dependent limiting shear stress friction model and material damage softening together. Above a value of 0.4, the model became unstable as the limiting shear stress was reduced significantly in the SDZ. Fig.10 also demonstrates that at a COF of 0.2 the contact is purely elastic due to the high limiting shear stresses, but at 0.4 this contact became fully plastic.

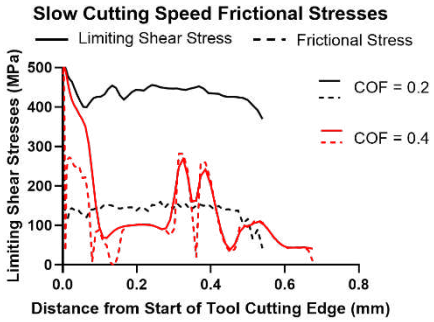

Fig. 10. The predicted limiting shear stresses (represented by the solid lines) and frictional shear stresses (represented by a dashed line) along the cutting edge and rake face of the tool.

5. Conclusions

A high-resolution experimental method was utilised to quantify local deformation filed within the PDZ and SDZ during an interrupted orthogonal cutting process. It is

demonstrated that the applied method can accurately determine material deformation history as well as local plastic strains at 20 μm proximity of the cutting tool rake face.

It is shown that a deformation dependent limiting frictional shear stress is necessary, assuming this to be a constant value and calculating this using the material uniaxial yield strength at the reference strain rate and temperature is not representative of the contact mechanics in the SDZ. The proposed model improves the physical meaning of the frictional shear stresses in the SDZ by incorporating the mechanics of deformation that change depending on the tool geometry, cutting conditions, and the material model. The model marginally improves the commonly under-predicted thrust force, although good agreement with the experimental cutting or thrust force could only be achieved separately at different manually tuned COF values, with a lower coefficient required to accurately predict the cutting force compared with the thrust force.

The limited benefit on the accuracy of the predicted forces is likely linked to the constant COF, which is not the case since the tribological condition of contact is not constant. Therefore, a more complex friction coefficient model is necessary that is dependent on the chip deformation and local tool-chip thermo-mechanical interaction properties, such as the temperature and relative velocity.

Acknowledgements

This work has been supported by Sandvik Coromant and grant # EP/L016257/1 from UK EPSRC.

References

[1] T. Özel, “The influence of friction models on finite element simulations of machining,” *Int. J. Mach. Tools Manuf.*, vol. 46, no. 5, pp. 518–530, 2006.

[2] A. J. Haglund, H. A. Kishawy, and R. J. Rogers, “An exploration of friction models for the chip-tool interface using an Arbitrary Lagrangian-Eulerian finite element model,” *Wear*, vol. 265, no. 3–4, pp. 452–460, 2008.

[3] F. Klocke, H. W. Raedt, and S. Hoppe, “2D-FEM simulation of the orthogonal high speed cutting process,” *Mach. Sci. Technol.*, vol. 5, no. 3, pp. 323–340, 2001.

[4] T. Mabrouki, F. Girardin, M. Asad, and J. F. Rigal, “Numerical and experimental study of dry cutting for an aeronautic aluminium alloy (A2024-T351),” *Int. J. Mach. Tools Manuf.*, vol. 48, no. 11, pp. 1187–1197, 2008.

[5] S. Kato, K. Yamaguchi, and M. Yamada, “Stress Distribution at the Interface Between Tool and Chip in Machining,” *J. Eng. Ind.*, vol. 94, no. 2, p. 683, 1972.

[6] L. Filice, F. Micari, S. Rizzuti, and D. Umbrello, “A critical analysis on the friction modelling in orthogonal machining,” *Int. J. Mach. Tools Manuf.*, vol. 47, no. 3–4, pp. 709–714, 2007.

[7] P. J. Arrazola and T. Özel, “Investigations on the effects of friction modeling in finite element simulation of machining,” *Int. J. Mech. Sci.*, vol. 52, no. 1, pp. 31–42, 2010.

[8] S. Subbiah and S. N. Melkote, “Effect of finite edge radius on ductile fracture ahead of the cutting tool edge in micro-cutting of Al2024-T3,” *Mater. Sci. Eng. A*, vol. 474, no. 1–2, pp. 283–300, 2008.

[9] R. T. Coelho, E. G. Ng, and M. A. Elbestawi, “Tool wear when turning hardened AISI 4340 with coated PCBN tools using finishing cutting conditions,” *Int. J. Mach. Tools Manuf.*, vol. 47, no. 2, pp. 263–272, 2007.

[10] T. H. C. Childs, “Friction modelling in metal cutting,” *Wear*, vol. 260, no. 3, pp. 310–318, 2006.

[11] T. H. C. Childs, P. J. Arrazola, P. Aristimuno, A. Garay, and I. Sacristan, “Ti6Al4V metal cutting chip formation experiments and modelling over a wide range of cutting speeds,” *J. Mater. Process. Technol.*, vol. 255, no. July 2017, pp. 898–913, 2018.

[12] S. Atlati, B. Haddag, M. Nouari, and M. Zenasni, “Thermomechanical modelling of the tool-workmaterial interface in machining and its implementation using the ABAQUS VUINTER subroutine,” *Int. J. Mech. Sci.*, vol. 87, pp. 102–117, 2014.

[13] F. Zemzemi, J. Rech, W. Ben Salem, A. Dogui, and P. Kapsa, “Identification of a friction model at tool/chip/workpiece interfaces in dry machining of AISI4142 treated steels,” *J. Mater. Process. Technol.*, vol. 209, no. 8, pp. 3978–3990, 2009.

[14] J. Rech, P. J. Arrazola, C. Claudin, C. Courbon, F. Pusavec, and J. Kopac, “Characterisation of friction and heat partition coefficients at the tool-work material interface in cutting,” *CIRP Ann. - Manuf. Technol.*, vol. 62, no. 1, pp. 79–82, 2013.

[15] F. Klocke, D. Trauth, A. Shirobokov, and P. Mattfeld, “FE-analysis and in situ visualization of pressure-, slip-rate-, and temperature-dependent coefficients of friction for advanced sheet metal forming: development of a novel coupled user subroutine for shell and continuum discretization,” *Int. J. Adv. Manuf. Technol.*, vol. 81, no. 1–4, pp. 397–410, 2015.

[16] S. N. Melkote *et al.*, “Advances in material and friction data for modelling of metal machining,” *CIRP Ann. - Manuf. Technol.*, vol. 66, no. 2, pp. 731–754, 2017.

[17] B. Thimm, A. Glavas, M. Reuber, and H. J. Christ, “Determination of chip speed and shear strain rate in primary shear zone using digital image correlation (DIC) in linear-orthogonal cutting experiments,” *J. Mater. Process. Technol.*, vol. 289, p. 116957, 2021.

[18] J. C. Outeiro, S. Campocasso, L. A. Denguir, G. Fromentin, V. Vignal, and G. Poulachon, “Experimental and numerical assessment of subsurface plastic deformation induced by OFHC copper machining,” *CIRP Ann. - Manuf. Technol.*, vol. 64, no. 1, pp. 53–56, 2015.

[19] G. List *et al.*, “Wear behaviour of cemented carbide tools in dry machining of aluminium alloy,” *Wear*, vol. 259, no. 7–12, pp. 1177–1189, 2005.

[20] B. Haddag, S. Atlati, M. Nouari, and M. Zenasni, “Analysis of the heat transfer at the tool–workpiece interface in machining: determination of heat generation and heat transfer coefficients,” *Heat Mass Transf. und Stoffuebertragung*, vol. 51, no. 10, pp. 1355–1370, 2015.

[21] S. Atlati, B. Haddag, M. Nouari, and A. Moufki, “Effect of the local friction and contact nature on the Built-Up Edge formation process in machining ductile metals,” *Tribol. Int.*, vol. 90, pp. 217–227, 2015.

[22] S. Atlati, A. Moufki, M. Nouari, and B. Haddag, “Interaction between the local tribological conditions at the tool–chip interface and the thermomechanical process in the primary shear zone when dry machining the aluminum alloy AA2024–T351,” *Tribol. Int.*, vol. 105, no. October 2016, pp. 326–333, 2017.